HHS Public Access

Author manuscript

J Phys Chem C Nanomater Interfaces. Author manuscript; available in PMC 2017 March 03.

Published in final edited form as:

J Phys Chem C Nanomater Interfaces. 2016 March 3; 120(8): 4546–4555. doi:10.1021/acs.jpcc.6b00185.

Multimodal Nonlinear Optical Imaging of Live Cells Using Plasmon-Coupled DNA-Mediated Gold Nanoprism Assembly

Sudarson Sekhar Sinha, **Stacy Jones**, **Teresa Demeritte**, **Suhash Reddy Chavva**, **Yongliang Shi**, **Jasmine Burrell**, **Avijit Pramanik**, and **Paresh Chandra Ray**

Department of Chemistry and Biochemistry, Jackson State University, Jackson, MS, USA; Fax: +16019793674

Paresh Chandra Ray: paresh.c.ray@jsums.edu

Abstract

Multiphoton excitation microscopy techniques are the emerging nonlinear optical (NLO) imaging methods to watch the biological world due its ability to penetrate deep into living tissues. Driven by the need to develop multimodal NLO imaging probe, current article reports the design of DNA-mediated gold nanoprisms assembly based optical antennas to enhance multiphoton imaging capability in biological II window. Reported experimental data show a unique way to enhance second harmonic generation (SHG) and two-photon fluorescence (TPF) properties by several orders of magnitudes via plasmon coupled organization into gold nanoprism assembly structures. Experimental and theoretical modeling data using finite difference time domain (FDTD) simulations indicate that huge enhancement of SHG and TPF properties are mainly due to the electric quadrupole contribution and electric field enhancement. Using 1100 nm biological II window light, reported results demonstrated that antibody conjugated assembly structures are capable of exhibiting highly selective and very bright multimodal SHG and TPF imaging of human Hep G2 liver cancer cells.

Graphical Abstract

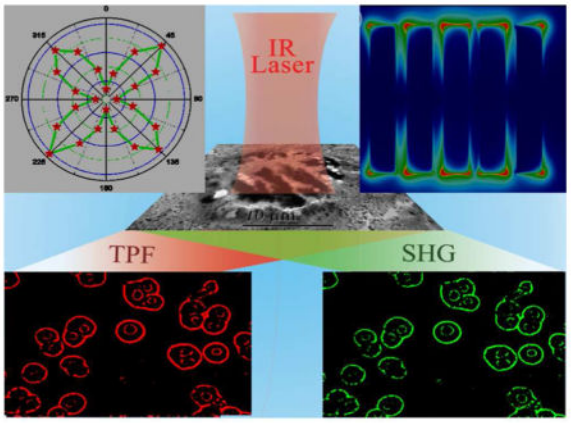

Correspondence to: Paresh Chandra Ray, paresh.c.ray@jsums.edu.

INTRODUCTION

Multiphoton microscopy via coupling of nonlinear optics (NLO) and scanning microscopy has opened up the possibility of new discovery for breakthrough in biology [1–10]. NLO imaging using second harmonic generation (SHG) and two-photon luminescence (TPL) are the emerging techniques to watch the biological world due its ability to penetrate deep into living tissue [11–20]. In last one decade, due to the huge advances in the innovative developments of laser systems, detector devices and optical filter design, we are now able to use the combination of several NLO modalities for advancing biological imaging into a single microscope platform, which is known as multimodal NLO imaging [21–30]. For *in vivo* imaging using noninvasive technology, near infrared (NIR) light between 650–950 nm (biological I window) and 1000–1350 nm (biological II window) needs to be used for providing maximum radiation penetration through tissue [1–5,11–13,31–33]. To date, most of the cell imaging is reported using biological I window (650–950 nm) NIR light, although it is well documented that due to the substantial background noise from tissue autofluorescence and the tissue penetration depth is limited to 1–2 cm, biological I window is not optimal[1–5,11–13]. However, due to the lack of available biocompatible probes in biological II window, clinical research has prevented the use of this highly sensitive spectral range for cancer imaging where one could improve signal-to-noise ratios by over 100-fold[1–5,11–13]. Driven by the need, this article reports the design of a DNA-mediated nanoprism assembly which has the capability for multimodal nonlinear optical SHG and TPL imaging using biological II window excitation light. Since the size of our design nanoparticle assembly is comparable to the wavelength of excitation NIR light, the higher-order multipolar resonances of plasmonic nanostructure will be able to couple with the free space incident electromagnetic field[3,7,10,18–20] and as a result, we have utilized the multipolar mode with the dipolar mode to cooperatively enhance the SHG and TPF processes simultaneously.

Second harmonic generation from nanoparticle is a nonlinear optical phenomena in which two same frequency (ω) photons interact with a nano-surface and produce a new photon with twice the frequency (2ω) [3,7,10,15–20], as shown in Scheme 1. In the last decade, SHG microscopy has become an emerging technique for biological and medical imaging and can be one of the alternative ways to improve penetration depth and decrease scattering and excitation volume[3,7,10,15–20]. Unfortunately, the technology for bio-imaging is currently limited due to poor signal-to-noise ratio resulting from the low second harmonic generation efficiency of available SHG probes. [3,7,10,15–20] Also, targeted live cell imaging is another huge issue. On the other hand, in case of two-photon fluorescence (TPF), nanoparticle or organic molecules absorb(s) two photons at a low energy state and emits a single excited photon at an energy level higher than that of the absorbed photons [4,5,11,13,32–33]. The imaging brightness for TPF microscope depends on the two-photon absorption cross-section and two-photon quantum yield of the probe[4,5,11–13,32–33]. However, finding a photo-stable two photon probe that exhibits strong two-photo luminescence efficiency in biological window II is rare[4,5,11–13,32–33].

Triangular-like gold nanoprisms possess strong electric field enhancement on the tip and exhibit high photo-stability and biocompatibility and as result, they are very good candidates for bio-imaging using a two-photon microscope [3,11,34–39]. In nano-assembly, due to the

presence of strong multipolar mode (l >1) band with dipolar mode (l=0), one can utilize both models to enhance optical properties [10,15–20]. Since two-photon nonlinear processes are inherently weak, we used plasmon coupling enhanced two-photon process for very bright imaging of cancer cells. For gold nanoprism, when light interacts in the surface, it couples with free-electron excitations near the surface and produces surface plasmon polaritons[3,11,34–39]. Due to the strong electromagnetic fields developed by the light confinement on the surface and lightning rod effect at the corner[3,11,34–39], weak two photon process can be significantly increased by 4–6 orders of magnitude. For further huge enhancement of two photon nonlinear processes, we have developed plasmon-coupled DNA mediated nano-assembly where plasmonic nanostructures are in close proximity. Due to the above fact, the electric field in the “hot spots” present between two nanoprism junctions is enhanced by several orders of magnitude. Since the two-photon optical properties is directly proportional to the fourth power of the fundamental field amplitude, an enhancement of 10^1 of the local field at the fundamental frequency for assembly structure will lead to an increase of up to 10^4 of the two-photon NLO properties. Our experimental findings are supported by finite difference time domain (FDTD) simulation [40–42] investigation, where we have included the multipolar and finite size effects in our calculation.

Despite huge advances in the cancer diagnosis research, cancer remains one of the leading causes of morbidity and mortality worldwide for human’s life [10–12,22,43–44]. Even in the 21st century, 5-year survival rate from liver cancer is around 5%.[43–44] To facilitate the use of NLO imaging tools in biological research, here we demonstrate the DNA mediated nano-assembly as an-efficient two-photon probe which can be used for targeted multiphoton multimodal for liver cancer cell imaging. Since Glypican-3 (GPC3) is significantly over-expressed in human Hep G2 liver cancer cell line [43–44], for selective binding and accurate NLO imaging, we have designed GPC3 specific monoclonal anti-GPC3 antibody attached nanoprisms assembly. Our reported result shows that bio-conjugated assembly can be used for NLO multimodal imaging live cancer cell using multiphoton microscope. To demonstrate the selectivity, identical experiments were performed using GPC3 (−) normal skin HaCaT and prostate cancer LNCaP cells.

EXPERIMENTAL SECTION

Hydrogen tetrachloroaurate, CTAB, KI, buffer, tri-sodium citrate and hydrogen tetrachloroaurate were obtained from Sigma-Aldrich. ss-DNA strands with –SH modification were purchased from Midland Certified Reagent. All cancer cells and normal cells including *Hep G2* liver cancer cells and HaCaT cell lines were purchased from the American Type Culture Collection (ATCC, Rockville, MD).

Synthesis and Characterization

Development of Gold Nanorpism—Triangular gold nanoprisms (60 ± 10 nm edge length, 5.5 ± 0.5 nm thick) were synthesized using seeded mediated growth method, as we and others have reported before [34–39]. In the first step, gold seeds were prepared by the reduction of $HAuCl_4$ in the presence of sodium thiosulfate ($Na_2S_2O_3$) as reducing agent. For this purpose, 20 mL of 2.5×10^{-4} M $HAuCl_4$ and 3.5×10^{-4} M trisodium citrate were added

to 0.4 mL of ice-cold 0.1 M $NaBH_4$ and 0.4 mL 0.1 M $Na_2S_2O_3$ solution. After that, the mixture was vigorously stirred for 2 min. A JEM-2100F transmission electron microscope (TEM) and UV–visible absorption spectrum were used for the characterization gold seeds and the average particle size of our developed seed was 3–4 nm. In the next step, gold nanoprisms were developed from gold seed in the presence of 1 mL of 0.1 M sodium thiosulfate ($Na_2S_2O_3$), 0.2 mL of 0.1 M KI and 1 mL of 0.1 M cetyltrimethylammonium bromide (CTAB) as capping agent. A JEM-2100F transmission electron microscope (TEM) and UV–visible absorption spectrum were used for the characterization of triangular gold nanoprisms, as shown in Figure 1.

Development of DNA-mediated Gold Nanorpism Assembly—DNA-mediated triangular gold nanoprisms assembly was designed using SH-modified dsDNA as a coupling agent. For this purpose, in the first step, thiolated ss-DNA molecules (HS–$(CH_2)_6$–ATTAGCACTG) were conjugated to triangular gold nanoprisms, followed by a passivation layer of thiolated polyethylene glycol. In the next step, assembly structures were developed using a complementary sequence (Oligo–$(CH_2)_6$–SH) attached triangular gold nanoprisms in 10 mM PBS solution containing 0.3 M NaCl. In the next step, assembly structures were separated from monomer via centrifugation at 1500 rpm for 20 minutes and then thoroughly washed using buffer. After that, the assembly structures were confirmed using DLS, TEM and absorption techniques.

Development of anti-GPC3 Antibody Conjugated Gold Nanoprisms Assembly —For targeted imaging of human *Hep G2* liver cancer cells, gold nanoprisms assembly were attached with anti-GPC3 antibody. To accomplish this, gold nanoprisms assembly structures were coated by amine modified polyethylene glycol (NH_2- PEG) initially. After PEGylation, anti-GPC3 antibody was attached with amine functionalized PEG coated gold nanoprism assembly using glutaraldehyde spacer method, as we have reported before [10,14].

Two-Photon Spectra Intensity Measurement—We used HRS technique to measure the two-photon scattering intensity from DNA-mediated triangular gold nanoprisms assembly and only nanoprism. Experimental details has been reported before[3,10,14,40]. For TPS and TPF intensity measurement, the fundamental 1100 and 1300 nm excitation light was generated using optical parametric amplifier (OPO), pumped by 100 fs pulse width and 80 MHz repetition rate Ti:sapphire laser (Coherent, USA). For the measurement of TPS signal only, we have used a high-pass filter, 3 nm bandwidth interference filter In this way, we are able to remove single photon Rayleigh scattering signal, two-photon fluorescence and higher order nonlinear optical signals from triangular gold nanoprisms assembly. For angle resolved TPS measurement from triangular gold nanoprisms or their assembly structure, we have used rotating half-wave plate to vary the angle of polarization.

Multimodal and Multi-Photon Imaging of Human Hep G2 Liver Cancer Cells—Two-photon multimodal TPF and SHG imaging of human *Hep G2* liver cancer cells using 1100 nm light was performed using anti-GPC3 antibody conjugated gold nanoprisms assembly attached human *Hep G2* liver cancer cells. For this purpose we used Olympus FV1000 MPE BX61 multi-photon microscope, as we have reported before [10,13,22,32].

Theoretical Calculation using Finite Difference Time Domain (FDTD) Simulation—For electromagnetic wave calculations, we used FDTD simulation software package, as previously reported by us and other groups[10,40–42]. Frequency dependent dielectric function of gold was used for the gold nano-antenna made from gold nanoprism assembly. To mimic experimental outcome, we have used experimental excitation wavelength for excitation of gold nano-antenna. The amplitude of electric field was kept as 1V/m and courant number was taken as 0.99. The entire simulation is done with 0.001 nm mesh resolution and 4000 fs time for all cases, as we have reported before [10,13,39].

Cell Culture—GPC3 (+) human *Hep G2* liver cancer cells and GPC3 (−) normal skin HaCaT cells were grown in 75-cm^2 tissue culture flasks according to the ATCC procedure. Experimental details have been reported before [10,13,22,32].

Cell Viability Assay—To determine the cytotoxicity of anti-GPC3 antibody attached gold nanoprisms assembly, different numbers of human Hep G2 liver cancer cells and normal skin HaCaT cells were incubated with anti-GPC3 antibody attached gold nanoprisms assembly separately. After two days of incubation the cell viability was determined using the MTT (3-(4,5-dimethylthiazol-2-yl)-2,5-diphenyltetrazolium bromide) assay and typan blue assay, as we have reported before [10,13,39].

RESULTS AND DISCUSSIONS

Triangular gold nanoprisms (60 ± 10 nm edge length, 5.5 ± 0.5 nm thick) were synthesized using seeded mediated growth method, as we and others have reported before [34–39]. In the first step, gold seeds were prepared by the reduction of $HAuCl_4$ in the presence of sodium thiosulfate ($Na_2S_2O_3$) as reducing agent. In the next step, gold nanoprisms were developed from gold seed in the presence of sodium thiosulfate ($Na_2S_2O_3$), KI and cetyltrimethylammonium bromide (CTAB) as capping agent. A JEM-2100F transmission electron microscope (TEM) and UV–visible absorption spectrum were used for the characterization of triangular gold nanoprisms, as shown in Figure 1. Figure 1A reports the mouphology of our triangular gold nanoprisms measured by TEM which are 50 ± 10 nm edge length and 5.5 ± 0.5 nm thick. As reported in Figure 1D, the extinction spectra shows two well developed bands. The strong one is the in-plane dipole band with $\lambda_{max} \approx 1300$. The weaker one at $\lambda_{max} \approx 800$ nm is quadrupole band, as reported before [34–39].

In the next step, DNA-mediated triangular gold nanoprisms assembly was designed using SH-modified dsDNA as a coupling agent. For this purpose, in the first step thiolated ss-DNA molecules (HS–$(CH_2)_6$–ATTAGCACTG) were conjugated to triangular gold nanoprisms, followed by a passivation layer of thiolated polyethylene glycol. In the next step, assembly structures were developed using a complementary sequence (Oligo–$(CH_2)_6$–SH) attached triangular gold nanoprisms in 10 mM PBS solution containing 0.3 M NaCl. After that, assembled structures were separated from monomer via centrifugation at 1500 rpm for 20 minutes and then thoroughly washed using buffer. Next, the assembly structures were confirmed using dynamic light scattering (DLS), TEM and absorption techniques. Since it is well documented that TEM grid preparation can increase aggregation [8–13], we have used DLS measurement to find the size of assembled structure in solution. To find the

reproducibility of designing assembly structure, we have performed the same experiment 5 times using freshly prepared gold nanoprism made at different batches. In all cases we have kept the concentration of DNA and gold nanoprism unaltered. Using DLS measurement, we have found out that the average size of the assembly structure is about 500–800 nm in each time, which is reproducible. TEM image as shown in Figures 1B–C also indicate the size is about 500–800 nm. As shown in Figures 1B and C, our experimental data clearly show face-to-face interactions are predominant between the gold nanoprisms and it is due to the fact that face-to-face interaction condition satisfies the maximizing interparticle DNA hybridization events. Figure 1D shows the extinction spectra for triangular gold nanoprisms assembly, which clearly shows that the dipole band became very broad and red shifted. Since in the assembly structure, gold nanoprisms are in close contact, due to the strong plasmon coupling between plasmon frequency of each gold nanoprism, extinction at longer wavelengths increases tremendously. The quadrupole band also became broad and slightly red shifted.

For the measurement of two-photon spectra (SHG or two-photon scattering and TPF signal together) from triangular gold nanoprisms assembly, we have used 1100 nm NIR biological II window light. On the other hand, for angle dependent two-photon scattering (TPS) measurement, we have used hyper Rayleigh scattering (HRS) technique [3, 20–24, 45–46] as we and others have reported before [3,10,13]. Excitation light was generated using optical parametric amplifier (OPO), pumped by 100 fs pulse width and 80 MHz repetition rate Ti:sapphire laser (Coherent, USA). Experimental details were reported before [10,13,22]. Two-photon signal was recorded using CCD camera (Princeton Instrument) integrated with a monochromator. Next, for the measurement of TPS signal only, we have used a high-pass filter, 3 nm bandwidth interference filter. In this way, we are able to remove single photon Rayleigh scattering signal, two-photon fluorescence and higher order nonlinear optical signals from triangular gold nanoprisms assembly. For angle resolved TPS measurement from triangular gold nanoprisms or their assembly structure, the fundamental beam at 1100 nm was linearly polarized, whereas the input angle of polarization was selected using a rotating half-wave plate.

To understand whether any photodamage occurs for the DNA-mediated triangular gold nanoprisms assembly or nanoprism itself, during first hyperpolarizability measurement using femto second laser, we have also performed TEM and DLS experiment before and after the β measurement which indicated no photothermal damage during HRS data collection time. Figure 2A shows the two-photon spectrum from DNA-mediated triangular gold nanoprisms assembly recorded for an excitation laser wavelength at 1100 nm. Our reported data clearly show that the DNA-mediated triangular gold nanoprisms assembly exhibit a strong TPS peak at 550 nm and a slightly weaker and broader TPF peak with λmax = 700 nm. On the other hand, no TPF or TPS peak was observed at 1100 nm excitation, when only DNA was used. As shown in Figure 2A, since there is no overlap between TPS and TPF peaks, reported experimental results indicate that we can easily eliminate contribution from TPF in the recorded SHG signal. Figure 2B shows that the TPS signal intensity from DNA-mediated triangular gold nanoprisms assembly exhibit a linear relationship with the square of the powers of the fundamental 1100 nm incident light, which clearly implies that the signal is indeed due to the two-photon process. Figure 3A shows how 550 nm two-photon

scattering (TPS) intensity varies due to the formation of DNA-mediated triangular gold nanoprisms assembly. Reported data clearly indicates that the two-photon scattering intensity from DNA-mediated triangular gold nanoprisms assembly are more than three order of magnitudes higher than for gold nanoprisms alone, which is highly remarkable.

To elucidate the origin of very high TPS intensity from DNA-mediated triangular gold nanoprisms assembly with respect to the gold nanoprism alone, we have performed angle resolved two-photon scattering measurement using 1100 nm incident light. For this prupose, we have used linearly polarized fundamental beam. We have used a rotating half-wave plate to change the angle of polarization. As per dipolar approximation, for cubic metals like gold, should not exhibit two-photon or second harmonic process, as we and others have reported before [3,9,14,19–25]. Now in case of plasmonic triangular nanoprism systems, surfaces will play a major role in generating strong two-photon scattering at 550 nm from imperfect metallic nanostructure surfaces[3,14,19–25]. On the other hand, for DNA-mediated triangular gold nanoprisms assembly, symmetry is broken at interfaces and as a result, TPS intensity will be much stronger for assembly structure. Since the size of the triangular gold nanoprisms usually of 50 ± 10 nm edge length, are quite small compared to the excitation wavelength of 1100 nm ($d \ll \lambda/10$), the TPS properties for triangular gold nanoprisms alone can be explained using the framework of electric-dipole approximation[3,9,14,19–30]. Our angle resolved two-photon scattering measurement, as reported in Figures 3C and 3D, clearly show that for the 50 ± 10 nm edge length triangular gold nanorpsim, the two photon scattering intensity response is governed by the electric-dipolar contribution. Whereas, in case of DNA-mediated gold nanoprism assembly structure, since the size is bigger than one tenth of the wavelength of 1100 nm incident light, contribution of higher-multipoles like electric quadrupole becomes very important for the two photon scattering spectra. As shown in Figure 3D, the polar plots for the TPS signal from DNA-mediated gold nanoprism assembly structure as a function of the angle of polarization, clearly show evidence of the deficiency of the electric-dipole approximation for nano-antenna system. As shown in Figure 3D, Instead of two lobes, we have observed four lobes which are oriented on the 45°, 135°, 225°, and 315° axes. Reported experimental data clearly demonstrate the presence of higher multipolar interactions in case of DNA-mediated gold nanoprism assembly system.

Since there is strong plasmon coupling in the DNA-mediated gold nanoprism assembly, to understand the role of plasmon coupling on the observed huge TPS intensity of assembly structure, we have performed full-wave simulations based on numerical solutions of Maxwell's equations, using the finite difference time domain (FDTD) simulation package, as we and others have reported before [10,40–42]. To mimic the experimental observation, in our simulations we have included multipolar and finite size effects, which is very important for assembly structure. FDTD simulation results from monomer, dimer, trimer and assembly of gold nanoprism, are illustrated in Figure 4. Reported data indicates more than 30 times of $|\boldsymbol{E}|^2$ intensity enhancement at the "hot spots" present between two nanoprism junctions for gold nanoprism assembly containing five particles in comparison to the monomer. As we have discussed before, the probability TPS signal intensity from nanorpism or its assembly, is proportional to the fourth power of the electric field enhancement. As a result, due to the formation of assembly structure, TPS intensity should increase around three orders of

magnitude just due the stronger electric field enhancement, as FDTD simulation data indicated. All the above experimental and theoretical data indicate that observed very strong two photon intensity from the DNA-mediated gold nanoprism assembly can be due to several factors. The first contribution can be due to the electric dipole contribution from gold nanoprism alone due to the imperfect structure of nanoprism and due to the broken symmetry at the interface of assembly system.

The second contribution can be due to electric quadrupole contribution which is due to the size of DNA-mediated gold nanoprism assembly. The third contribution can be due to the electric field enhancement via strong plasmon coupling in the DNA-mediated gold nanoprism assembly. The fourth contribution for very strong TPS intensity from DNA-mediated gold nanoprism assembly is single photon plasmon resonance. To understand the contribution of plasmon resonance in the observed TPS intensity, we have also performed two-photon experiment using 1300 nm light. Measured two-photon intensity indicates that the TPS intensity increases about 2.1 times with comparison to 1100 nm excitation. This clearly indicates that plasmon resonance plays important role for enhance TPS intensity. As shown in Figure 2A, DNA-mediated triangular gold nanoprisms assembly exhibit strong and very broad TPF signal and as a result, it can be used as TPF imaging material. Figure 2C shows that the TPF signal intensities at 700 nm, from DNA-mediated triangular gold nanoprisms assembly exhibit a linear relationship with the square of the powers of the fundamental 1100 nm incident light, which clearly implies that the signal is indeed due to the two-photon fluorescence process. Figure 3B reports the TPF spectra from DNA-mediated triangular gold nanoprisms assembly and triangular gold nanoprisms alone, when they have been excited using 1100 nm NIR light. Reported experimental data indicate that the TPF signal from gold nanoprism assembly structures are about 4 order magnitudes higher than that of monomer gold nanoprism alone. The plasmon frequency amplified tremendously in assembly nanostructures, due to the strong coupling between each gold nanorpism. FDTD data as reported in Figure 4 also confirmed it. Since during TPL measurement we have used 1100 nm excitation wavelength, which is in resonance with the DNA-mediated triangular gold nanoprisms assembly, single photon resonance will have contribution in our observed huge TPL intensity enhancement. To understand the contribution of plasmon resonance in the observed TPF intensity, we have also measured the TPF intensity using 1300 nm light. Measured two-photon intensity indicates that the TPF intensity increases about 3.1 times with comparison to 1100 nm excitation. This clearly indicates that plasmon resonance plays an important role in enhancing TPF intensity.

As our experimental data show that DNA-mediated triangular gold nanoprism assembly exhibit very high SHG and TPF properties, it can be an excellent material for multimodal two-photon bio-imaging. To demonstrate that DNA-mediated triangular gold nanoprisms assembly can be used as two-photon imaging probe for targeted multimodal imaging, a well-characterized human Hep G2 liver cancer cell, which expresses a high level of glypican-3 (GPC3) antigen relative to normal cells [43–44], has been used. Since glypican-3 (GPC3) is significantly over-expressed in human Hep G2 liver cancer cell line for selective binding and accurate two-photon imaging, we have designed GPC3 specific monoclonal anti-GPC3 antibody attached gold nanoprisms assembly for selective imaging of human Hep G2 liver cancer cell. To find out whether anti-GPC3 antibody attached gold nanoprisms assembly

based two-photon multimodal imaging is highly selective or not, we have also performed experiments with GPC3 negative human skin HaCaT keratinocytes. To understand the biocompatibility and photo-stability, we have performed initially the biocompatibility and photo-stability experiment for anti-GPC3 antibody attached gold nanoprisms assembly. The experimental data as reported in Figure 2D, clearly indicate that TPS signal at 550 nm remain almost unchanged even after an hour of illumination, which shows very good photo-stability for anti-GPC3 antibody attached gold nanoprisms assembly as SHG imaging material.

Similarly, as reported in Figure 5A, our experimental data clearly show very good photo-stability for anti-GPC3 antibody attached gold nanoprisms assembly as a TPF imaging material. Next, to understand the biocompatibility of anti-GPC3 antibody attached gold nanoprisms assembly, 3.4×10^5 cells/mL of human Hep G2 liver cancer cells were incubated with anti-GPC3 antibody attached gold nanoprisms assembly for different time intervals up to 50 hours. To determine the cell viability, we have used trypan blue assay where living cells are colorless due to unable to bind with trypan blue. On the other hand, since dead cells are able to bind with the blue dye all dead cells with will be blue color and as a result, cell viability was qualitatively determined from the color of the cell monolayer. We have also used the MTT test which is a colorimetric assay for assessing cell metabolic activity to determine the number of live cells. As reported in Figures 5B–5D, experimental data clearly show that even after two days of incubation with anti-GPC3 antibody attached gold nanoprisms assembly more than 97% cell viability was observed for human Hep G2 liver cancer cells and more than 98% cell viability was noted for normal human skin cell line. All the above reported results clearly indicate very good biocompatibility of anti-GPC3 antibody attached gold nanoprisms assembly.

Due to good biocompatibility, two-photon properties and photo-stability, we have used anti-GPC3 antibody attached gold nanoprisms assembly for multimodal SHG and TPF microscopy imaging contrast agent for *Hep G2* liver cancer imaging. For this purpose, initially anti-GPC3 antibody attached gold nanoprisms assembly were incubated with different concentrations of human Hep G2 liver cancer cells cells for 40 minutes. Next, after 40 minutes of incubation, unconjugated human Hep G2 liver cancer cells were separated using centrifugation followed by washing with buffer.

We performed centrifugation followed by washing with buffer four times to make sure that all the unattached with anti-GPC3 antibody conjugated gold nanoprisms assembly are separated from the solution. Figure 5E shows the high-resolution TEM image which indicates that that single *Hep G2 liver cancer* cell is conjugated with anti-GPC3 antibody conjugated gold nanoprisms assembly. After that, we have used Olympus FV1000 MPE BX61 multi-photon microscope for multimodal two-photon imaging of *Hep G2* liver cancer cells conjugated with anti-GPC3 antibody conjugated gold nanoprisms assembly. The SHG and TPF images for *Hep G2* liver cancer cells were taken 9 times to average for the best quality image. Figures 6 show very bright SHG and TPF image of *Hep G2* liver cancer cells which are conjugated with anti-GPC3 antibody conjugated gold nanoprisms assembly, when they are excited using 1100 nm light. The experimentally observed bright image clearly indicates that anti-GPC3 antibody conjugated gold nanoprisms assembly can be used for

very bright two-photon imaging of *Hep G2* liver cancer cells. Our reported two-photon imaging result as shown in Figures 6B and 6C, indicate that anti-GPC3 antibody conjugated gold nanoprisms assemblies are not only localized in proximity of the *Hep G2* liver cancer cell membrane, they have also penetrated through the cell membrane and localized inside the cell. Several reported data show that gold nanoparticle of different shapes can be internalized into cells either via the classic endocytic and nonendocytotic pathways [39,47–48]. Since the size of anti-GPC3 antibody conjugated gold nanoprisms assembly is quite big, the endocytosis pathway will be the most probable path by which the assembly structure can enter inside the cell. To understand the fate of the nanoprism assemblies after imaging, we have measured the cell viability of *Hep G2 liver cancer* cell attached nanoasembly using MTT test. Experiments have been performed at different time intervals after the two-photon imaging experiment. We found that cell that the viability remains almost unchanged even after 12 hours. To understand nano-assemblies total clearance and greater toxicological evaluation, animal model experiments need to be performed, which is our future goal.

Next, to find out whether anti-GPC3 antibody conjugated gold nanoprisms assembly based two-photon imaging is selective for *Hep G2* liver cancer cells, we hperformed the same experiment with GPC3 (−) normal skin HaCaT cells. For this purpose, anti-GPC3 antibody conjugated gold nanoprisms assembly were incubated with 4.6×10^5 cells/mL normal skin HaCaT cells for 60 minutes. In the next step, unconjugated anti-GPC3 antibody conjugated gold nanoprisms assembly were separated by centrifugation After that, we have performed SHG imaging of normal skin HaCaT cells which indicate non-targeted HaCaT normal skin cells do not bind with anti-GPC3 antibody conjugated gold nanoprisms assembly. As a result, anti-GPC3 antibody conjugated gold nanoprisms assembly based SHG and TPF multimodal imaging of *Hep G2* liver cancer cells is highly selective for targeted cell.

CONCLUSION

In conclusion, we have reported the development of plasmon coupled DNA-mediated gold nanoprisms assembly for multimodal two-photon SHG and TPF multimodal imaging of live cancer cells. We demonstrate the effectiveness of DNA-mediated nanoparticle antennas to enhance multimodal multiphoton imaging capability. Reported experimental data show a unique way to increase SHG and TPF properties of gold nanoprisms by several orders of magnitudes via plasmon coupled organization into assembly structures using DNA as coupling agent. SHG and TPF measurement from plasmon coupled DNA-mediated gold nanoprisms assembly demonstrated that two-photon nonlinear optical properties can be enhanced four orders of magnitude, by developing DNA based assembly structure. The huge enhancement of two-photon properties in DNA based nanoprism assembly structure is due to the electric quadrupole contribution and electric field enhancement via strong plasmon coupling. Our theoretical modeling data using FDTD simulations indicate that four orders of magnitude enhancement of two-photon properties are mainly due to plasmon resonance enhancement coupled with huge electric field enhancement. Experimental observation shows anti-GPC3 antibody conjugated gold nanoprisms assembly exhibits very good photo-stability and cellular biocompatibility. Two-photon multimodal liver cancer cells imaging observation in the second biological NIR window shows that anti-GPC3 antibody conjugated gold nanoprisms assembly is capable for multimodal two-photon SHG and TPF

imaging of human ***Hep G2*** **liver cancer** cells selectively. Although our reported data show promising advances for antibody conjugated gold nanoprisms assembly as selective multimodal multiphoton cancer cell imaging, we are till now in infancy in how to control the nanoprism assembly architecture in clinical sample environment to stabilize and maximize the imaging capability for clinical study.

Acknowledgments

Dr. Ray thanks NSF-PREM grant # DMR-1205194 for their generous funding. We are grateful for use of the JSU Analytical Core Laboratory–RCMI facility supported by NIH grant # G12MD007581.

References

1. Weisslede R, Nahrendorf W. Advancing Biomedical Imaging. Proc Natl Acad Sci U S A. 2015; 112:14424–14428. [PubMed: 26598657]
2. Kim HM, Cho BR. Small-Molecule Two-Photon Probes for Bioimaging Applications. Chem Rev. 2015; 115:5014–5055. [PubMed: 25938620]
3. Ray PC. Size and Shape Dependent Second Order Nonlinear Optical Properties of Nanomaterials and their Application in Biological and Chemical Sensing. Chem Rev. 2010; 110:5332–5365. [PubMed: 20469927]
4. Hoover EE, Squier JA. Advances in Multiphoton Microscopy Technology. Nature Photon. 2013; 7:93–101.
5. Welsher K, Yang H. Multi-resolution 3D Visualization of the Early Stages of Cellular Uptake of Peptide-coated Nanoparticles. Nat Nanotechnol. 2014; 9:198–203. [PubMed: 24561356]
6. Murphy CJ, Vartanian AM, Geiger FM, Hamers RJ, Pedersen J, Cui Q, Haynes CL, Carlson EE, Hernandez R, Klaper RD, et al. Biological Responses to Engineered Nanomaterials: Needs for the Next Decade. ACS Central Science. 2015; 1:117–123. [PubMed: 27162961]
7. Pantazis P, Maloney J, Wu D, Fraser SE. Second Harmonic Generating (SHG) Nanoprobes for in Vivo Imaging. Proc Natl Acad Sci US A. 2010; 107:14535–14540.
8. Bogart LK, Pourroy G, Murphy CJ, Puntes V, Pellegrino T, Rosenblum D, Peer D, Levy R. Nanoparticles for Imaging, Sensing, Therapeutic Intervention. ACS Nano. 2014; 8:3107–3122. [PubMed: 24641589]
9. Cox JD, Garcia de Abajo FJ. Electrically Tunable Nonlinear Plasmonics in Graphene Nanoislands. Nat Commun. 2014; 5:5725–5730. [PubMed: 25500534]
10. Demeritte T, Fan Z, Sinha SS, Duan J, Pachter R, Ray PC. Gold Nanocage Assembly for Selective Second Harmonic Generation Imaging of Cancer Cell. Chem—Eur J. 2014; 20:1017–1022. [PubMed: 24339156]
11. Chinen AB, Guan CM, Ferrer JR, Barnaby SN, Merkel TJ, Mirkin CA. Nanoparticle Probes for the Detection of Cancer Biomarkers, Cells, and Tissues by Fluorescence. Chem Rev. 2015; 115:10530–10574. [PubMed: 26313138]
12. Xu H, Li Q, Wang L, He Y, Shi J, Tang B, Fan C. Nanoscale Optical Probes for Cellular Imaging. Chem Soc Rev. 2014; 43:2650–2661. [PubMed: 24394966]
13. Tchounwou C, Sinha SS, Viraka BP, Pramanik A, Kanchanapally R, Jones S, Chavva SR, Ray PC. Hybrid Theranostic Platform for Second Near-IR Window Light Triggered Selective Two-Photon Imaging and Photothermal Killing of Targeted Melanoma Cells. ACS Appl Mater Interfaces. 2015; 7:20649–20656. [PubMed: 26327304]
14. Lu W, Arumugam SR, Senapati D, Singh AK, Arbneshi T, Khan SA, Yu H, Ray PC. Multifunctional Oval Shape Gold Nanoparticle Based Selective Detection of Breast Cancer Cells Using Simple Colorimetric and Highly Sensitive Two-Photon Scattering. ACS Nano. 2010; 4:1739–1749. [PubMed: 20155973]
15. Meer B, Gui L, Fuchs J, Floess D, Hentschel M, Giessen H. Strong Enhancement of Second Harmonic Emission by Plasmonic Resonances at the Second Harmonic Wavelength. Nano Lett. 2015; 15:3917–3922. [PubMed: 25867489]

16. Dong Z, Asbahi M, Lin J, Zhu D, Wang YM, Hippalgaonkar K, Chu HS, Goh WP, Wang F, Huang Z, et al. Second-Harmonic Generation from Sub-5 nm Gaps by Directed Self-Assembly of Nanoparticles onto Template-Stripped Gold Substrates. Nano Lett. 2015; 15:5976–5981. [PubMed: 26270086]
17. Czaplicki R, Mäkitalo J, Siikanen R, Husu H, Lehtolahti J, Kuittinen M, Kauranen M. Second-Harmonic Generation from Metal Nanoparticles: Resonance Enhancement Versus Particle Geometry. Nano Lett. 2015; 15:530–534. [PubMed: 25521745]
18. Sorger VJ, Zhang X. Physics. Spot Light on Plasmon Lasers. Science. 2011; 333:709–710. [PubMed: 21817040]
19. Butet J, RussierAntoine I, Jonin C, Lascoux N, Benichou E, Brevet PF. Sensing with Multipolar Second Harmonic Generation from Spherical Metallic Nanoparticles. Nano Lett. 2012; 12:1697–1701. [PubMed: 22375818]
20. Alkilany AM, Lohse SE, Murphy CJ. The Gold Standard: Gold Nanoparticle Libraries to Understand the Nano-Bio Interface. Acc Chem Res. 2013; 46:650–661. [PubMed: 22732239]
21. Shi Y, Pramanik A, Tchounwou C, Pedraza F, Crouch RA, Chavva SR, Vangara A, Sinha SS, Jones S, Sardar D, et al. Multifunctional Biocompatible Graphene Oxide Quantum Dots Decorated Magnetic Nanoplatform for Efficient Capture and Two-photon Imaging of Rare Tumor Cells. ACS Appl Mater Interface. 2015; 7:10935–10943.
22. Butet J, Brevet PF, Martin OJF. Optical Second Harmonic Generation in Plasmonic Nanostructures: From Fundamental Principles to Advanced Applications. ACS Nano. 2015; 9:10545–10562. [PubMed: 26474346]
23. Butet J, Bachelier G, Russier-Antoine I, Jonin C, Benichou E, Brevet PF. Interference between Selected Dipoles and Octupoles in the Optical Second-Harmonic Generation from Spherical Gold Nanoparticles. Phys Rev Lett. 2010; 105:077401–077404. [PubMed: 20868074]
24. Zhang Y, Grady NK, Ayala-Orozco C, Halas NJ. Three-Dimensional Nanostructures as Highly Efficient Generators of Second Harmonic Light. Nano Lett. 2011; 11:5519–5523. [PubMed: 22043857]
25. Hanke T, Cesar J, Knittel V, Trügler A, Hohenester U, Leitenstorfer A, Bratschitsch R. Tailoring Spatiotemporal Light Confinement in Single Plasmonic Nanoantennas. Nano Lett. 2012; 12:992–996. [PubMed: 22268812]
26. Kruk S, Weismann M, Bykov AY, Mamonov EA, Kolmychek IA, Murzina T, Panoiu NC, Neshev DN, Kivshar YS. Enhanced Magnetic Second-Harmonic Generation from Resonant Metasurfaces. ACS Photonics. 2015; 2:1007–1012.
27. Biwas S, Liu X, Jarrett JW, Brown D, Pustovit V, Urbas A, Knappenberger KL Jr, Nealey PF, Vaia RA. Nonlinear Chiro-Optical Amplification by Plasmonic Nanolens Arrays Formed via Directed Assembly of Gold Nanoparticles. Nano Lett. 2015; 15:1836–1842. [PubMed: 25646978]
28. Celebrano M, Wu X, Baselli M, Grobmann S, Biagioni P, Locatelli A, De Angelis C, Cerullo G, Osellame R, Hecht B. Mode Matching in Multiresonant Plasmonic Nanoantennas for Enhanced Second Harmonic Generation. Nat Nanotechnol. 2015; 10:412–417. [PubMed: 25895003]
29. Singh A, Lehoux A, Remita H, Zyss J, Ledoux-Rak I. Second Harmonic Response of Gold Nanorods: A Strong Enhancement with the Aspect Ratio. J Phys Chem Lett. 2013; 4:3958–3961.
30. Butet J, Thyagarajan K, Martin OJF. Ultrasensitive Optical Shape Characterization of Gold Nanoantennas Using Second Harmonic Generation. Nano Lett. 2013; 13:1787–1792. [PubMed: 23458149]
31. Pramanik A, Chavva SR, Fan Z, Sinha S, Nellore BP, Ray PC. Extremely High Two-Photon Absorbing Graphene Oxide for Imaging of Tumor Cells in the Second Biological Window. J Phys Chem Lett. 2014; 5:2150–2154. [PubMed: 26270507]
32. Accanto N, Piatkowski L, Renger J, van Hulst NF. Capturing the Optical Phase Response of Nanoantennas by Coherent Second-Harmonic Microscopy. Nano Lett. 2014; 14:4078–4082. [PubMed: 24927109]
33. Singh AK, Senapati D, Neely A, Kolawole G, Hawker C, Ray CP. Nonlinear Optical Properties of Triangular Silver Nanomaterials. Chem Phys Lett. 2009; 481:94–98.

34. Millstone JE, Park S, Shuford KL, Qin LD, Schatz GC, Mirkin CA. Observation of a Quadrupole Plasmon Mode for a Colloidal Solution of Gold Nanoprisms. J Am Chem Soc. 2005; 127:5312–5313. [PubMed: 15826156]
35. Viarbitskaya S, Teulle A, Marty R, Sharma J, Girard C, Arbouet A, Dujardin E. Tailoring and Imaging the Plasmonic Local Density of States in Crystalline Nanoprisms. Nat Mater. 2013; 12:426–432. [PubMed: 23503011]
36. Zhou Y, Zhou X, Park DJ, Torabi K, Brown KA, Jones MR, Zhang C, Schatz GC, Mirkin CA. Shape-Selective Deposition and Assembly of Anisotropic Nanoparticles. Nano Lett. 2014; 14:2157–2161. [PubMed: 24661194]
37. Pelaz B, Grazu V, Ibarra A, Magen C, del Pino P, de la Fuente JM. Tailoring the Synthesis and Heating Ability of Gold Nanoprisms for Bio applications. Langmuir. 2012; 28:8965–8970. [PubMed: 22260484]
38. PérezHernández M, delPino P, Mitchell S, Moros M, Stepien G, Pelaz B, Parak WJ, Gálvez EM, Pardo J, de la Fuente JM. Dissecting the Molecular Mechanism of Apoptosis during Photothermal Therapy Using Gold Nanoprisms. ACS Nano. 2015; 9:52–61. [PubMed: 25493329]
39. Sinha SS, Paul DK, Kanchanapally R, Pramanik A, Chavva SR, Nellore BPV, Jones SJ, Ray PC. Long-range Two-photon Scattering Spectroscopy Ruler for Screening Prostate Cancer Cells. Chem Sci. 2015; 4:2411–2418.
40. Yan Y, Li L, Feng C, Guo W, Lee S, Hong M. Microsphere-Coupled Scanning Laser Confocal Nanoscope for Sub-Diffraction-Limited Imaging at 25 nm Lateral Resolution in the Visible Spectrum. ACS Nano. 2014; 8:1809–1816. [PubMed: 24471860]
41. Zhao J, Pinchuk AO, McMahon JM, Li S, Ausman LK, Atkinson AL, Schatz GC. Methods for Describing the Electromagnetic Properties of Silver and Gold Nanoparticles. Acc Chem Res. 2008; 41:1710–1720. [PubMed: 18712883]
42. [date of access 03/02/2015] http://www.cancer.org/cancer/livercancer
43. Zhang Y, Li J, Cao L, Xu W, Yin Z. Circulating Tumor Cells in Hepatocellular Carcinoma: Detection Techniques, Clinical Implications, and Future Perspectives. Semin Oncol. 2012; 39:449–460. [PubMed: 22846862]
44. Ishizuka T, Sinks LE, Song K, Hung ST, Clays K, Therien MJ. The Roles of Molecular Structure and Effective Optical Symmetry in Evolving Dipolar Chromophoric Building Blocks to Potent Octopolar Nonlinear Optical Chromophores. J Am Chem Soc. 2011; 133:2884–2896. [PubMed: 21322603]
45. Chandra M, Indi SS, Das PK. Depolarized Hyper-Rayleigh Scattering from Copper Nanoparticles. J Phys Chem C. 2007; 111:10652–10656.
46. Darbha GK, Rai US, Singh AK, Ray PC. Gold Nanorod-Based Sensing of Sequence-Specific HIV-1 Viris DNA by Using Hyper-Rayleigh Scattering Spectroscopy. Chem—Eur J. 2008; 14:3896–3903. [PubMed: 18348156]
47. Kostarelos K, Lacerda L, Pastorin G, Wu W, Wieckowski S, Luangsivilay J, Godefroy S, Pantarotto D, Briand JP, Muller S, et al. Cellular Uptake of Functionalized Carbon Nanotubes is Independent of Functional Group and Cell Type. Nat Nanotechnol. 2007; 2:108–113. [PubMed: 18654229]
48. Bhattacharya S, Roxbury D, Gong X, Mukhopadhyay D, Jagota A. DNA Conjugated SWCNTs Enter Endothelial Cells *via* Rac1 Mediated Macropinocytosis. Nano Lett. 2012; 12:1826–1830. [PubMed: 22375622]

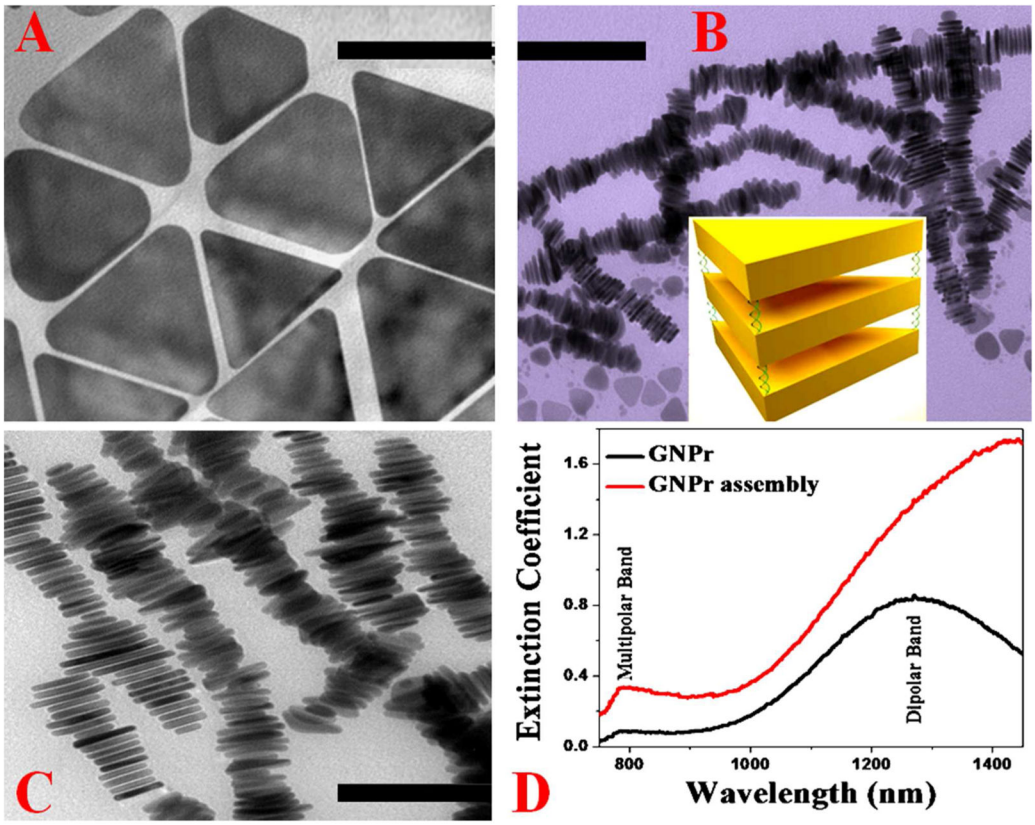

Figure 1.

TEM image of freshly prepared triangular gold nanoprisms (50 ± 10 nm edge length, 5.5 ± 0.5 nm thick) (scale bar = 40 nm). B) TEM image of freshly prepared DNA mediated gold nanoprism assembly before separation (scale bar = 200 nm). It clearly shows that most triangular gold nanoprisms are in assembly structure via face-to-face linking between the 2D nanoprisms. Inserted diagram shows how triangular gold nanoprisms are in assembly structure via face-to-face connection via DNA. C) TEM image of freshly prepared DNA mediated gold nanoprism assembly after separation via centrifuging at 1500 rpm for 20 minutes followed by thorough washing to remove unreacted triangular gold nanoprisms (scale bar = 100 nm). D) Extinction spectra of monomer and DNA-mediated triangular gold nanoprisms. For triangular gold nanoprisms monomer, an in-plane dipole band with $\lambda_{max} \approx$ 1300 nm and a quadrupole band with $\lambda_{max} \approx$ 800 nm were observed. For triangular gold nanoprisms assembly, the dipole band became very broad and red shifted. The quadrupole band also became broad and slightly red shifted for assembly structure.

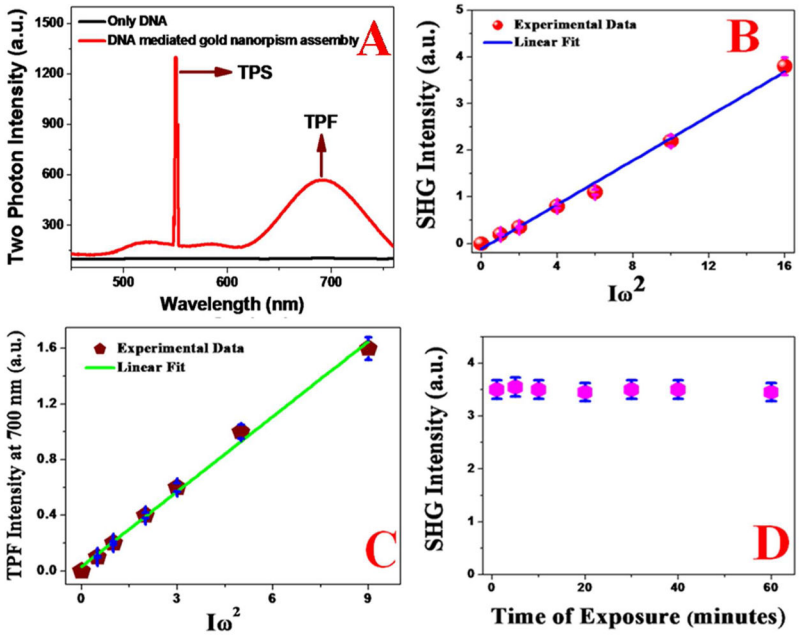

Figure 2.

A) Two-photon emission spectrum from DNA-mediated gold nanoprism assembly at 1100 nm excitation. Spectrum shows a strong TPS peak at 550 nm and broad two-photon luminescence with emission maxima at 700 nm. Two-photon emission spectrum from DNA at 1100 nm excitation, shows no observable TPS and TPF peaks. B) Plot shows linear relationship between SHG intensity at 550 nm from DNA-mediated gold nanoprism assembly and the square of intensity of 1100 nm excitation laser power, which clearly indicates that it is a two-photon process. C) Plot shows linear relationship between TPF intensity at 700 nm from DNA-mediated gold nanoprism assembly and the square of intensity of 1100 nm excitation laser power, which clearly indicates that it is a two-photon fluorescence process. D) Plot shows the photostability of TPS intensity at 550 nm from DNA-mediated gold nanoprism assembly.

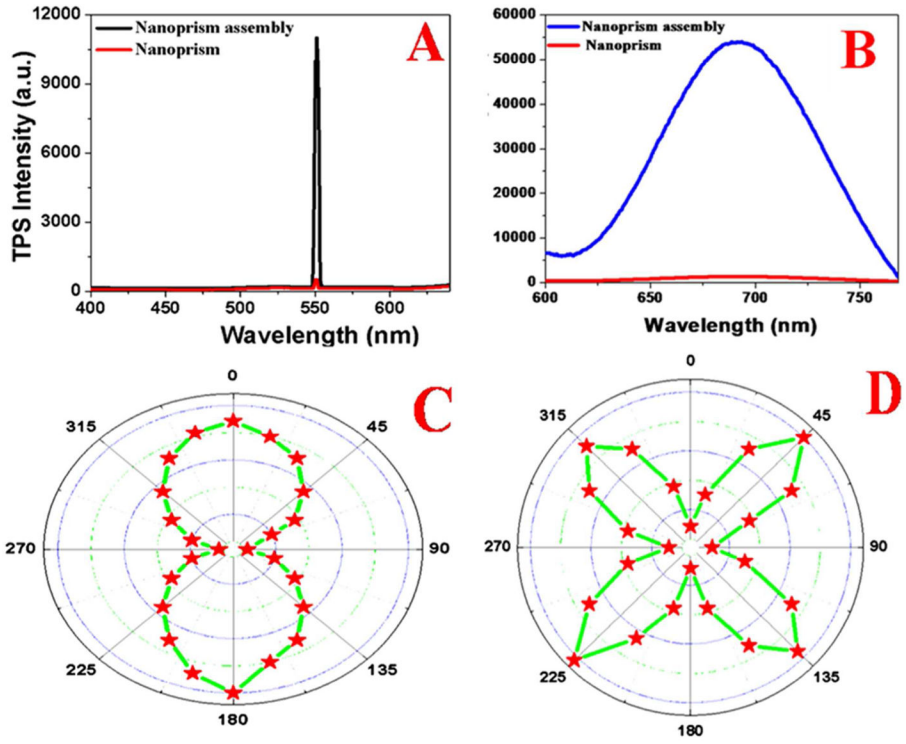

Figure 3.

A) Two-photon scattering spectrum from freshly prepared DNA-mediated gold nanoprism assembly and comparison with only gold nanoprism. We have used 1100 nm light as an excitation source. Plot clearly shows that enhancement of more than three orders of magnitude of two-photon scattering intensity due to the formation of DNA-mediated gold nanoprism assembly. B) Two-photon-fluorescence spectrum from freshly prepared DNA-mediated gold nanoprism assembly in comparison with only gold nanoprism. We have used 1100 nm light as excitation source. Plot clearly shows that enhancement of more than two orders of magnitude of two-photon fluorescence intensity due to the formation of DNA-mediated gold nanoprism assembly. C, D) Plot shows how the two photon scattering intensity varies with the fundamental light angle of polarization, C) monomer gold nanoprism and D) DNA-mediated gold nanoprism assembly.

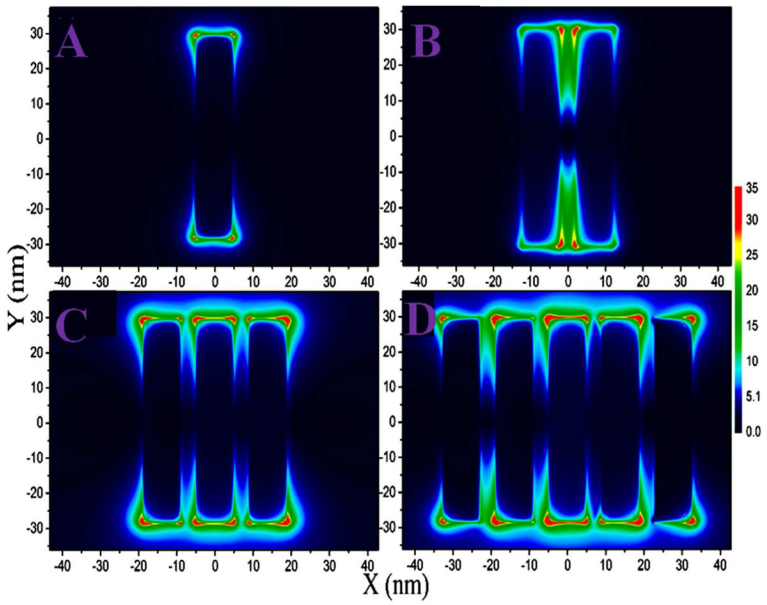

Figure 4.

Plot shows FDTD simulated electric field enhancement $|E|^2$ profiles (arb. unit) for monomer, dimer and gold nanoprism assembly structure. Since our experimental data clearly show that face-to-face interactions are predominant between the gold nanoprisms in the assembly structure, we have used experimentally observed structure in our calculation. For our calculation, we have used gold nanoprisms with 50 nm edge length and 5 nm thickness, as observed in our experimental data. The separation distance between gold nanoprisms are kept as 3 nm.

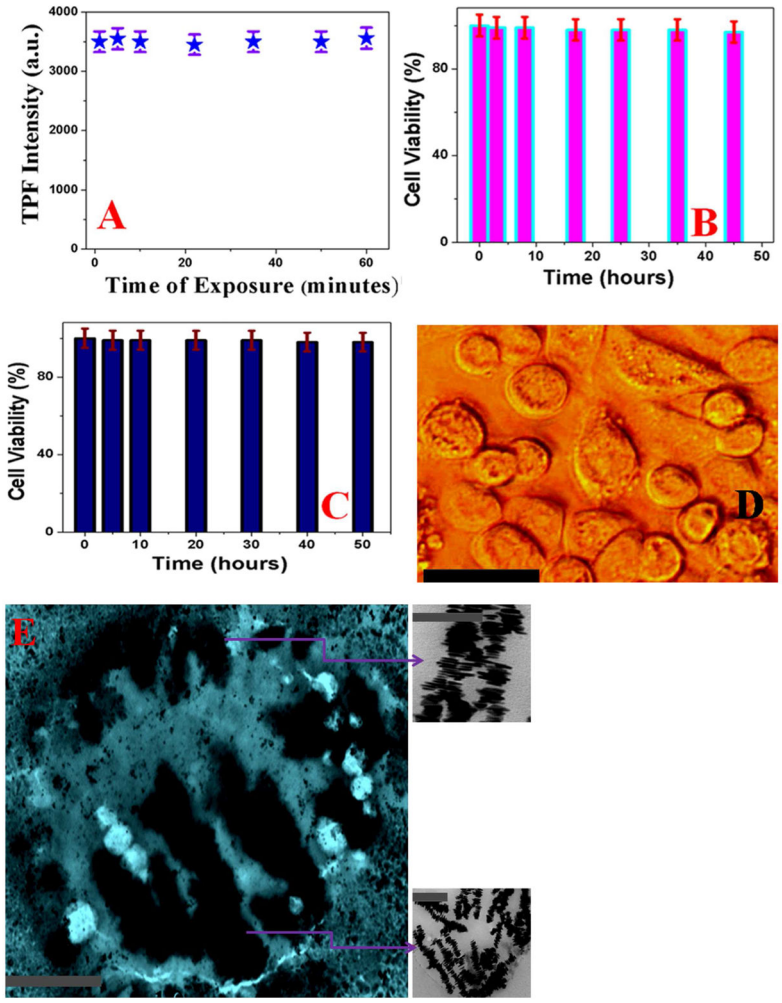

Figure 5.

A) Plot shows the photo-stability of TPF intensity at 700 nm from anti-GPC3 antibody attached DNA-mediated gold nanoprism assembly even after an hour of exposure with 1100 nm light. B) Bar plot shows very good biocompatibility even after 48 hours incubation of anti-GPC3 antibody attached DNA-mediated triangular gold nanoprisms assembly against human Hep G2 liver cancer cells. After two days of incubation with human Hep G2 liver cancer cells, we have observed about 98% cell viability. C) Bar plot shows very good biocompatibility even after 50 hours incubation of anti-GPC3 antibody attached DNA-mediated triangular gold nanoprisms assembly against HaCaT normal skin cells. After more than two days of incubation with human HaCaT normal skin cells, we have observed about 97% cell viability. D) Bright-field inverted microscopic images of human Hep G2 liver cancer cells after 48 hours of incubation with anti-GPC3 antibody attached DNA-mediated triangular gold nanoprisms assembly. Reported data indicate that cancer cells are alive even after two days of incubation. (scale bar = 20 μm) E) TEM image shows single human Hep G2 liver cancer cell is conjugated with anti-GPC3 antibody attached nanoprisms assembly (scale bar = 1 μm). Inserted picture shows the morphology of anti-GPC3 antibody attached nanoprisms assembly on Hep G2 liver cancer cell surface (scale bar = 200 nm).

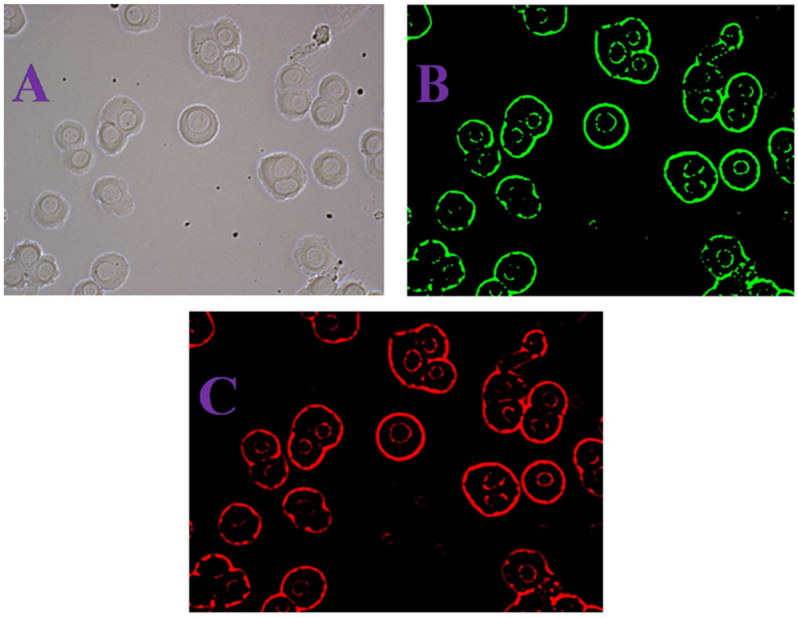

Figure 6.

A) Bright-field image of anti-GPC3 antibody attached gold nanoprisms assembly conjugated human Hep G2 liver cancer cells. B) SHG images of anti-GPC3 antibody attached gold nanoprisms assembly conjugated human Hep G2 liver cancer cells, at 1100 nm excitation. C) Two-photon fluorescent images of anti-GPC3 antibody attached gold nanoprisms assembly conjugated human Hep G2 liver cancer cells at 1100 nm excitation.

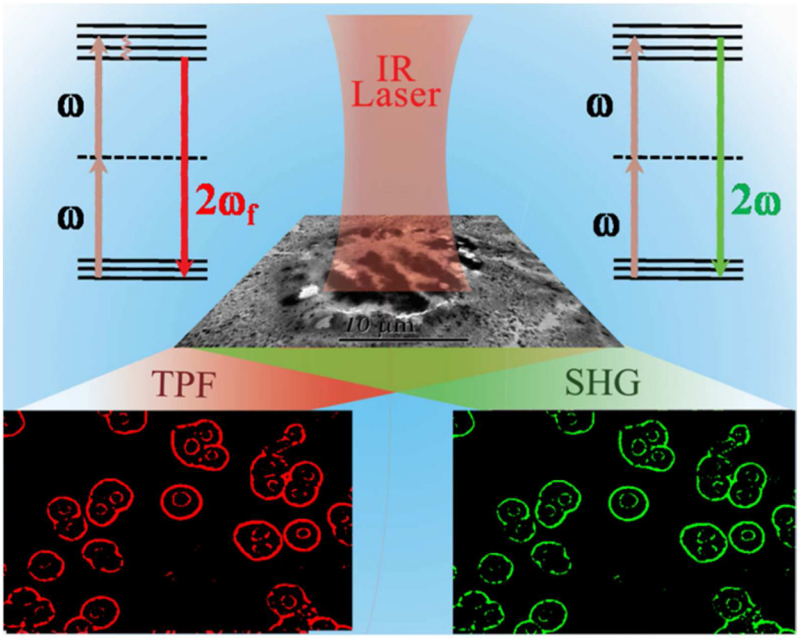

Scheme 1.

Schematic representation showing multimodal NLO imaging of human liver cancer cells using 1100 nm biological II window light.